Electrodynamic bare tether systems as a thruster for the Momentum-Exchange/Electrodynamic Reboost (MXER) project

G. V. Khazanov,[1] E. N. Krivorutsky,[2] and D. L. Gallagher[1]

Received 23 April 2005; revised 2 December 2005; accepted 12 January 2006; published 27 April 2006.

[1] The concept of electrodynamic tether propulsion has a number of attractive features and has been widely discussed for different applications. Different system designs have been proposed and compared during the last 10 years. In spite of this, the choice of proper design for any particular mission is a unique problem. Such characteristics of tether performance as system acceleration, efficiency, etc., should be calculated and compared on the basis of the known capability of a tether to collect electrical current. We discuss the choice of parameters for circular and tape tethers with regard to the Momentum-Exchange/Electrodynamic Reboost (MXER) tether project.

Citation: Khazanov, G. V., E. N. Krivorutsky, and D. L. Gallagher (2006), Electrodynamic bare tether systems as a thruster for the Momentum-Exchange/Electrodynamic Reboost (MXER) project, *J. Geophys. Res.*, *111*, A04309, doi:10.1029/2005JA011205.

1. Introduction

[2] Electrodynamic propulsion based on the interaction of a conducting tether with the background magnetic field can be implemented across a range of system designs. Bare tethers [*Sanmartin et al.*, 1993; *Estes et al.*, 2002], bare and insulated tethers with a balloon termination [*Vannaroni et al.*, 2000; *Sanmartin et al.*, 2001; *Ahedo and Sanmartin*, 2002], and insulated tethers with a grid-sphere termination [*Stone et al.*, 2002] have been suggested for different applications. An electrodynamic tether as a thruster is currently proposed for the Momentum-Exchange/Electrodynamic Reboost (MXER) tether facility that has the potential to provide a fully reusable in-space propulsion infrastructure and dramatically reduce propulsion cost for many space missions [*Hoyt*, 2000; *Sorensen*, 2003]. The MXER facility will consist of a rotating, ~100 km long tether with components distributed along its length. MXER is to be operated in an elliptical trajectory, where a payload in a low circular orbit is caught by the rotating tether, accelerated by its tension and released with a velocity about 2.4 km/s larger than the initial one. The electrodynamic component of MXER, the topic of this work, will be used to restore the system's kinetic energy lost to the boosted payload.

[3] In order for the tether system to boost multiple payloads, it must have the capability to restore its orbital energy and momentum after each payload transfer operation as rapidly as possible. A tether system that is positively biased relative to the ambient environment requires an anode contactor that will enable it to collect electrons from ionospheric plasma. Because active plasma contactors require expenditure of propellant and may require significant additional mass, the bare wire tether technology is also being considered for the MXER tether [*Hoyt et al.*, 2003]. However *Stone et al.* [2002] expressed a concern about self-shielding of the bare tether at the high current levels due to the formation of a magnetic field around the wire [*Khazanov et al.*, 2000; *Sanmartin and Estes*, 2002]. Such a field may have an impact on operation of tethers that flow large currents such as that required in the MXER concept.

[4] The choice of tether design for a specific mission is based on the analysis of tether system performance for the mission conditions. Different parameters describing tether performance, such as system acceleration and efficiency can be calculated, if the current distribution along the tether for the satellite trajectory is known. Below we present the results of efficiency calculations for the expected trajectory of the MXER tether using circular and tape cross sections and considering the possible magnetic shielding effects based on the results of *Khazanov et al.* [2001] and *Sanmartin and Estes* [2002].

2. Tether Current Collection Model

[5] The basic physics of bare tether current collection is well known. The detailed formulation of the problem is presented by *Sanmartin et al.* [1993], *Khazanov et al.* [2000, 2001], and *Sanmartin and Estes* [2002].

[6] In the tether's reference frame of rest exists an electric field, $\vec{E} = \vec{u} \times \vec{B}_o/c$, where $\vec{u}$ is the tether orbital velocity, c is the speed of light, and B_0 is the ambient magnetic field. The unperturbed potential, V_p, in plasma in the direction parallel to the wire is proportional to the projection of this electric field $\vec{E}$ on the tether direction, E_m, and $dV_p \sim E_m dz$. Here the z axis is chosen along the tether. The potential along the wire, V_t, changes in accordance with Ohm's law. Then for a local bias we have $\Delta V = V_t - V_p$ and for the thruster mode the local bias changes as

$$\frac{d\Delta V}{dz} = \frac{I}{\sigma S} + E_m \tag{1}$$

[1]NASA Marshall Space Flight Center, Huntsville, Alabama, USA.
[2]Universities Space Research Association, National Space Science and Technology Center, Huntsville, Alabama, USA.

0148-0227/06/2005JA011205$09.00

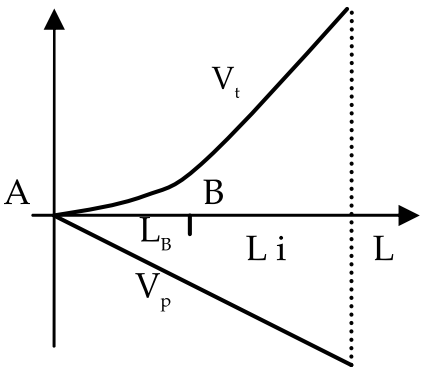

Figure 1. Schematics of voltage-tether length dependence.

where σ is the tether conductivity and S is the tether cross section. The equation for the OML current I along the tether is

$$\frac{dI}{dz} = en_e\varepsilon(l)G\frac{p}{\pi}\sqrt{\frac{2\Delta V}{m_e}} \tag{2}$$

Here: n_e is the unperturbed electron density; G and $\varepsilon(l)$ are correction coefficients that account for deviation from the standard OML theory due to large size and cross-section geometry of the tether (G) and the self-induced magnetic field ($\varepsilon(l)$); p is the tether perimeter or circumference. Both coefficients, $\varepsilon(l)$ and G, are dependent on system parameters, but the dependence on tether length (local bias) in G can be neglected [*Sanmartin and Estes*, 1999; *Estes and Sanmartin*, 2000]. Calculation of $\varepsilon(l)$ is presented by *Khazanov et al.* [2001]. In dimensionless variables [*Sanmartin et al.*, 1993]

$$l = \frac{z}{L^*}; \quad L^* = \left(\frac{m_eE_m}{2e}\left(\frac{3\pi\sigma S}{4Gepn_e}\right)^2\right)^{1/3}; \quad i = \frac{I}{\sigma SE_m}; \quad \phi = \frac{\Delta V}{E_mL^*} \tag{3}$$

equations (1) and (2) can be written as

$$\frac{di}{dl} = \frac{3}{4}\varepsilon(l)\sqrt{\phi}; \quad \frac{d\phi}{dl} = i + 1 \tag{4}$$

[7] The boundary condition for the current is $i_A = 0$ at the tether end A (Figure 1). It is also assumed that the potential at this point, $\phi_A = 0$, is maintained. Because the solution of the equations is completely determined by the boundary conditions at point A, the results describe the fully bare tether as well as the partly insulated one.

[8] Equations (3) and (4) will be used for the calculation of the magnetic shielding effect. For the tether efficiency analysis we will set the coefficient $\varepsilon(l)$ equal to one. It then follows from equations (4), for the chosen boundary conditions, that $\phi = (2i + i^2)^{2/3}$. This expression can be approximated with an error of about 5% for the current range $0 \le i \le 10$ as

$$\phi = 1.5i^{2/3}\left[1 + 0.4i - 0.045i^{2/3}(1 + 4i/7)\right] \tag{5}$$

With the help of this approximation the current collected by the bare tether segment between the point A and current point z can be expressed as a function of the normalized length of this segment l

$$i = \frac{1}{0.09^{3/2}}\left(1 - \sqrt{1 - 0.12l}\right)^{3/2} \tag{6}$$

3. Tether Performance

[9] It is expected that the MXER tether would operate in an equatorial elliptical orbit with perigee in the altitude range of 300–500 km and apogee in the range of 5000–10,000 km [*Sorensen*, 2003]. The specific orbit chosen would be a function of the tip velocity of the tether, which is in turn a function of the orbital transfer desired and the limitations of material tensile strength. We will consider a trajectory with perigee at 300 km altitude and an apogee of 8500 km. For such a trajectory, the electric field induced in the altitude range of 300–900 km is presented in Table 1. The angle between the satellite velocity and the Earth's magnetic field has been taken to be 90°. Table 1 also contains typical plasma densities during the day for different altitudes and the plasma temperature is taken to be 1900°K. The flight times starting from perigee are presented in the last column of Table 1. The orbital period of the facility motion is 3.06 hours and it rotates with the period about 400s [*Hoyt*, 2000].

[10] Tether performance can be characterized by the ratio of system mass, dedicated to thrust, M_d, to the product of thrust, F and thrust duration, τ, ($M_d/F\tau$). *Sanmartin et al.* [2001] have discussed this characteristic for an electrodynamic tether. In what follows, their approach will be adopted for this problem. The electrical and thrusting powers, W and W_t, needed for this ratio calculation can be found from equations (4) [*Sanmartin et al.*, 2001].

$$W = I[\Delta V_B + E_mL_B\delta(1 + i)]$$
$$W_t = Fv = (W/i) - \sigma SE_m^2L_B(1 + \delta) \tag{7}$$

Here ΔV_B is the bias at point B (Figure 1), and $\delta = L_i/L_B$, where the length of the bare tether segment AB is L_B, L_i is the length of the tether insulated part and v is the facility velocity. Equations (7) in the dimensionless form can be written as:

$$w = \frac{i_B}{1 + \delta}\left[\frac{\phi_B}{l_B} + \delta(1 + i_B)\right], \quad w_t = \frac{w}{i_B} - 1, \quad l_B = \frac{L_B}{L^*} \tag{8}$$

where $w(w_t) = W(W_t)/\sigma E_m^2LS$ and L is the total tether length. The normalized powers are dependent on two parameters, l_B and δ. During the facility transition through the ionosphere

Table 1. Plasma Parameters Along the Tether Trajectory

H, km	B_0, G	E, V/km	n_e, cm^{-3}, day	Flight Time, s
300	0.27	230	$1.6\cdot10^6$	0.0
400	0.26	220	$1.5\cdot10^6$	483
500	0.25	210	$9.0\cdot10^5$	688
600	0.24	200	$4.0\cdot10^5$	848
700	0.23	190	$2.0\cdot10^5$	987
800	0.22	180	$1.0\cdot10^5$	1112

for a given tether, l_B changes because of the dependence of the normalization length L^* (expression (3)) on the plasma density and on the induced electric field E_m along the tether. The prescribed energy, K_t, that should be delivered by the tether to restore the facility orbit during the prescribed time can be expressed as

$$K_t = NLS\sigma E_0^2 T \sum w_{tj}\left(\frac{E_{mj}}{E_0}\right)^2 \tau_j, \quad \tau_j = \frac{t_j}{T}, \quad T = \sum t_j \quad (9)$$

Here N is the number of revolutions defined by this prescribed time and facility orbital period, j identifies the altitude layers, t_j is the time of thrust during the transition through the layer, and E_0 is a normalizing electric field. The corresponding electrical energy required from the source, K, can be presented in the same way, by the substitution of $w_{tj} \rightarrow w_{tj}/\eta_j$ into equation (9) and by introducing the power efficiency η_j with the help of expressions (8). The average energy power efficiency is then

$$\eta = \frac{K_t}{K} = \frac{\sum w_{tj}\left(E_{mj}/E_0\right)^2 \tau_j}{\sum\left(w_{tj}/\eta_j\right)\left(E_{mj}/E_0\right)^2 \tau_j} \quad (10)$$

The mass dedicated to thrust consists of two terms, neglecting the mass of the propellant for the cathode contactor,

$$M = \beta\frac{K}{N} + \alpha M_t \quad (11)$$

The term K/N is the energy that should be produced, stored, and released during one orbital period. Instead of the required power [*Sanmartin et al.*, 2001], the required energy is used here for the calculation of dedicated mass (solar panels and batteries), because of the specifics of the problem. Energy is produced and stored during the flight outside the ionosphere and consumed at the time of the transition through it. For Scarlet-type solar panels and Li ion batteries with a maximum permitted depth-of-discharge of 30%, it has been found that $\beta \approx 6.7 \cdot 10^{-3}$ kg/kJ [*Hoyt*, 2000]. αM_t is the mass related to the tether mass M_t, where $\alpha = 2$–3 [*Sanmartin et al.*, 2001]. The impulse change due the thrust per one orbital period can be presented as

$$\sum F_j t_j = \frac{K_t}{Nv} \quad (12)$$

From equations (11) and (12)

$$\frac{M}{\sum F_j t_j} = v\beta\left[\frac{1}{\eta} + \frac{\gamma}{\sum w_{tj}\left(E_{mj}/E_0\right)^2 \tau_j}\right] = \frac{v\beta}{\eta_t} \quad (13)$$

Here $\gamma = \rho\alpha/\beta\sigma T E_0^2$ and ρ is the tether material density.

[11] Because of the facility rotation, we will assume that the tether operates only during half of the transition time through the ionosphere (Table 1). This is a good approximation owing to the large number of transitions through the ionosphere at varying tether angle to vertical. Reboost takes place over a time period much larger than the orbital period (~3 hours) and the facility rotation period (~400 s). The total time with the tether angle less than 45° (active reboost) during ionospheric transition averages to about half the total time in transition during the reboost phase. For such timescales we can also assume that any angle in the range 0° to 45° has equal probability during reboost. If the facility rotates in the orbital plane, this angle, ϑ_m, defines the projection of the induced electric field, $E_{mj} = E_j \cos\vartheta_m$, on the tether direction. We will use $\langle K\rangle$ and $\langle K_t\rangle$ in expressions (10)–(13) to characterize tether performance, where K and K_t are averaged over the possible angles between the tether and the vertical. In what follows the bare segment length $l_B(j, \vartheta_m)$ will be normalized by its value l_B at some reference point. The so normalized bare segment tether length is a function of the nonlinear ratios of the electric fields and plasma densities at a given position of interest and the fixed reference position. The reference position will be taken at 300 km altitude and the angle $\vartheta_m = 0°$ for defining the reference length, l_B. The normalized mass to total impulse ratio $\langle M/v\beta\sum F_j t_j\rangle = 1/\eta_t$ (black curves), electric energy efficiency, $\langle\eta\rangle$ (red curves), and normalized trust power, $\langle K_t/NLS\sigma E_0^2 T\rangle$ (blue curves) as functions of l_B for different ratios between the bare and insulated tether lengths, δ, are plotted in Figure 2. The constants used in this plot are as follows: $\alpha = 2.25$ [*Sanmartin et al.*, 2001], $\beta \approx 6.7 \cdot 10^{-3}$ kg/kJ [*Hoyt*, 2000], density and conductivity are taken for aluminum, other parameters are taken from Table 1, and the times are taken as half the values in Table 1 on the basis of the discussion above. In addition, these results are obtained under the condition that the bias at the bare end of the tether is held equal to zero.

[12] One of the restrictions on tether performance is imposed by the availability of source electrical potentials. A reasonable maximum potential is apparently 5 kV [*Hoyt*, 2000]. The potential drop along the tether can be calculated from equations (4) with constant current for the insulated tether segment, and it is largest (as is the current) at 300 km altitude in the ionosphere and for $\vartheta_m = 0°$

$$U = E_0 L_B\left[\frac{\phi_B}{l_B} + \delta(1 + i_B)\right] \quad (14)$$

The largest lengths of the tether bare segment permitted by the potential 5 KV as a function of l_B for different δ are presented in Figure 2 in green. The results plotted in Figure 2 are the same for circular and tape tethers for the same l_B and δ.

[13] The limitations imposed by the available source voltage (14), the choice of the ratio between the bare and insulated segment lengths, δ, and the choice of a certain l_B also defines the radius for the circular tether (expression (3)), as well as the maximum collected current, the thrust energy, and the consumed electrical energy during one orbital period. For the tape geometry this choice defines only the cross section to perimeter ratio, where the tape width and thickness can still vary. Note that the prescribed cross section to perimeter ratio also defines the minimal tape cross-section area, which is the cross section of a square. Within this limitation the tape cross section can be chosen to satisfy other requirements. We defined the cross section

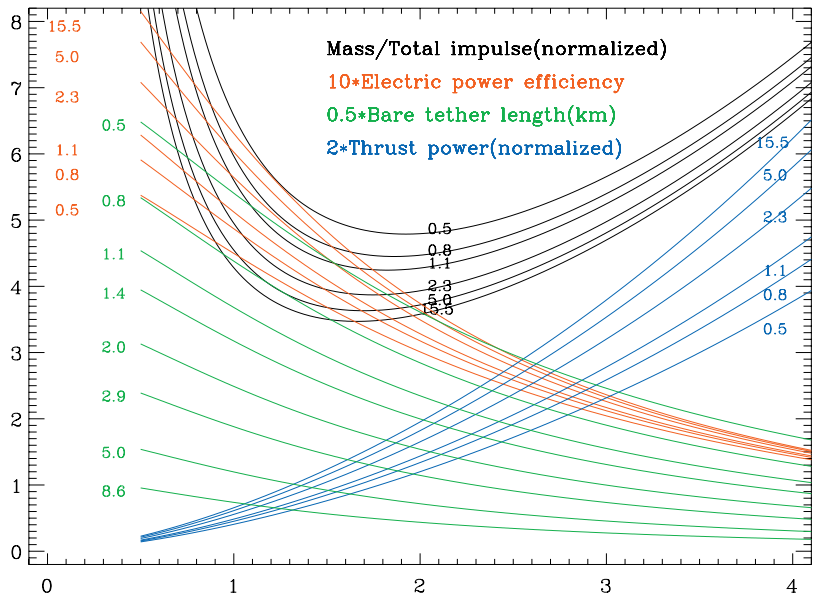

Figure 2. Normalized mass to total impulse ratio, $\langle 1/\eta_t \rangle$ (black curves); electric power efficiency, $\langle \eta \rangle$ (red curves); normalized thrust power, $\langle K_t/NLS\sigma {E_0}^2 T \rangle$ (blue curves); and bare segment tether length for different bare to insulated segments length ratios, δ, as functions of the normalized bare segment length, l_B.

prescribing the collected current at the reference conditions for which it is largest. This current and the choice of l_B define the tape thickness and width.

[14] For a circular tether the current and the tether radius are plotted as functions of l_B and δ in Figure 3a. The maximum considered current is taken to be 50A, and the permitted tether radius is restricted by the condition that it should be smaller than the plasma Debye length in the densest ionosphere layer (0.2 cm), which is the condition of validity of the OML approach. For the tape tether, Figures 3b and 3c present the tape width and the thickness for currents 25A and 50A. Additional conditions on the thickness, h, and the width of the tape, d, imposed by the OML theory validity, are taken as $h + d \leq 4\lambda_D \approx 1$ cm [*Sanmartin et al.*, 2001]. Note, that because of the prescribed source voltage, the choice of the current defines the maximum required source power.

[15] The available thrust work per one facility revolution $\langle K_t \rangle/N$ has been calculated under the conditions listed above (expression (9) averaged over facility rotation). Following *Hoyt* [2000] the payload capability is taken to be 2500 kg with the energy needed to restore the facility orbit after the payload launch equal to 54 GJ. The thrust work, $\langle K_t \rangle/N$, normalized to the work per facility revolution that is needed to restore the position of the MXER facility within 100 days after launch (68.9 MJ) is presented in Figures 4a–4c. The red curves in Figures 4a–4c present the corresponding tethers mass. Note that for prescribed l_B and δ this work, $\langle K_t \rangle/N$, is dependent only on the tether volume SL, while the available l_B and δ are dependent on the chosen current and the tether cross-section geometry. Because $\langle K_t \rangle/N$ for the chosen l_B and δ depends only on the tether volume to obtain the required work, the same mass is needed for tethers with circular and rectangular cross sections.

[16] The domain of the tether parameters presented in Figures 3 and 4 is also restricted by the requirements that the electrical energy efficiency $\langle \eta \rangle \geq 0.2$, and the normalized work $\langle K_t \rangle/N$ is larger then 0.01.

4. Discussion and Conclusion

[17] Figures presented above characterize the performance of a tether with a specific design or can be used to find the tether parameters needed for the desired performance. The black curves in Figure 2, presenting the mass to total impulse ratio $1/\eta_t$ near the minimum, i.e., in the region of interest, slightly depend on the ratio between the insulated and bare segments length, δ, if it is large enough. The same is true for the electric energy efficiency (red curves), η. This permits the ratio to be chosen so as to satisfy other requirements. Both quantities insignificantly change if the current is collected only at altitudes up to 600 km compare to 800 km. For the first range of altitudes the required electrical power changes ~2.5 times. While the electrical power efficiency, η, is nearly unaffected by the tether rotation, the mass to total impulse ratio, $1/\eta_t$, is enlarged by the rotation, because of the dependence of γ on T in expression (13). For a rotating system T has been taken two times smaller than in Table 1. $1/\eta_t$ is ~75% lower for the minimum and about two times smaller for $l_B \sim 0.8$ if the system rotation is suppressed. Blue curves presenting the normalized trust energy, $\langle K_t/NLS\sigma E_0^2 T \rangle$, also characterize the trust energy per unit tether mass.

[18] As can be seen from Figure 3a, permitted values for l_B at a given δ are restricted by the maximum considered current for larger l_B, and by the condition of applicability of the OML approach for the smaller values. Normalized work is presented in Figure 4a (black curves) for values of l_B at which both conditions are satisfied. This thrust work normalized to the energy that is needed to restore the position of the MXER facility during 100 days after the launch (68.9 MJ) in Figure 3a, even in the maximum, is less

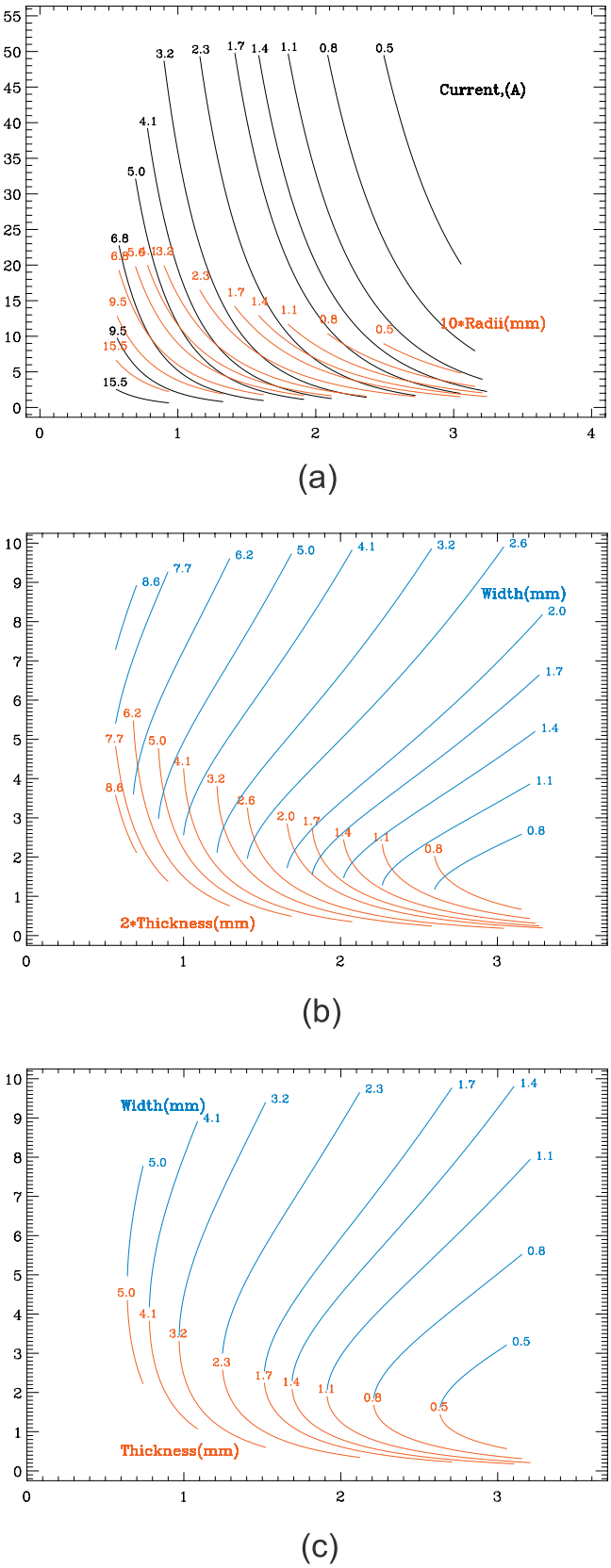

Figure 3. (a) Currents and tether radii and tape width and thickness for currents (b) 25A and (c) 50A, respectively, as functions of l_B for different δ.

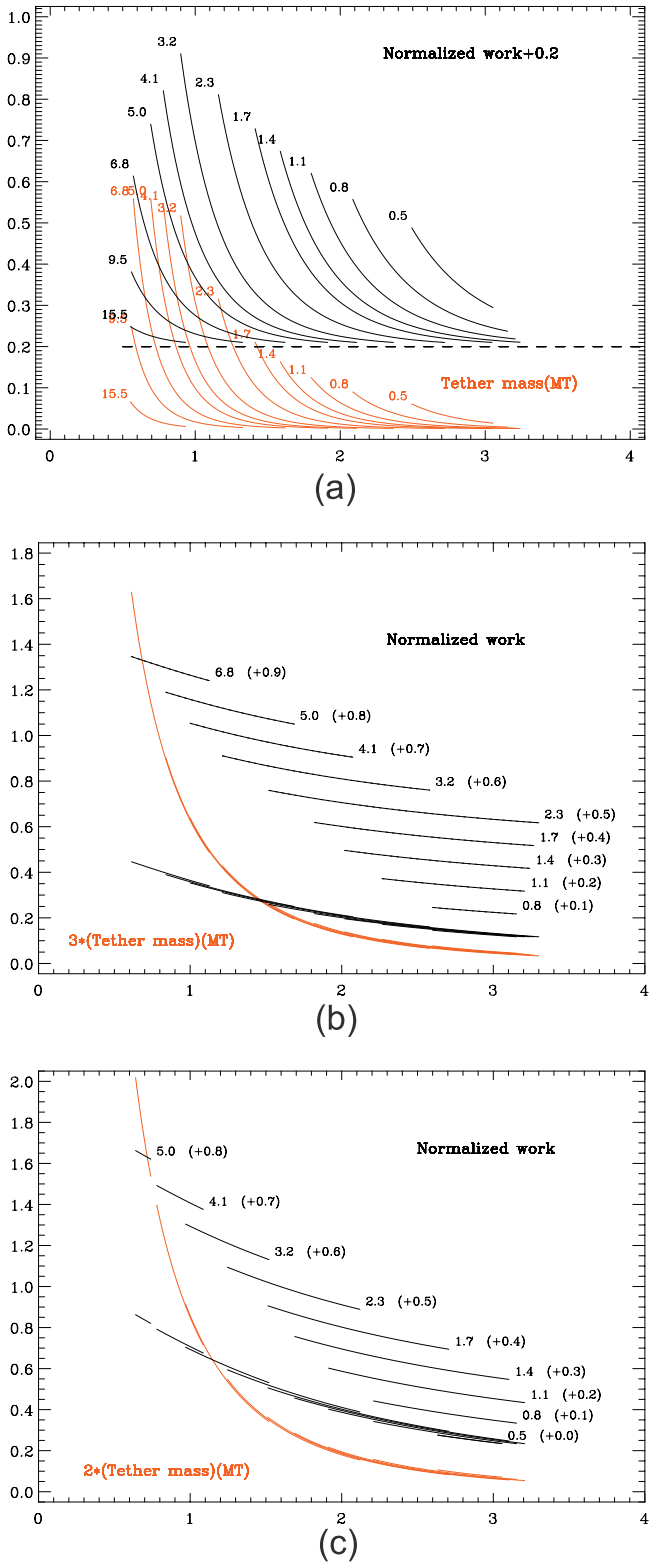

Figure 4. Thrust work for one revolution normalized to 68.85 MJ and tether mass for (a) circular and rectangular cross sections ((b) current 25A and (c) current 50A) as functions of l_B for different δ.

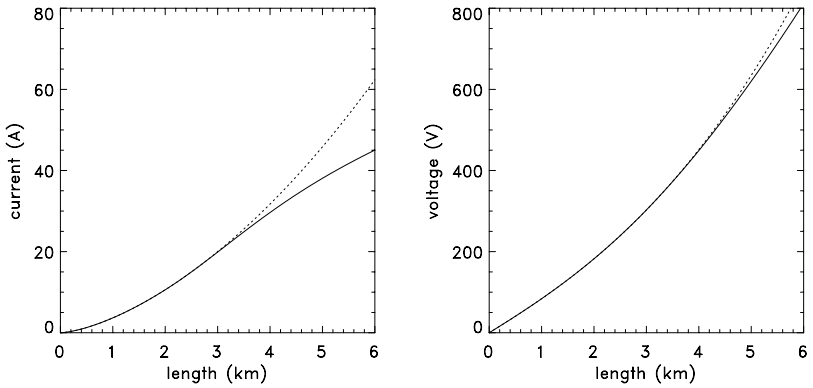

Figure 5. Current and local bias distributions as functions of the bare tether segment length with the magnetic shielding (solid lines), and neglecting it, for nonequatorial trajectory; r_w = 2.0 mm, n_e = $1.6 \cdot 10^6$ cm^{-3}, E_m = 80 V/km, and B_0 = 0.25 G.

than unity and therefore more than one tether is needed under the imposed restrictions. Depending on the chosen ratio between the bare and insulated segments length, δ, for a chosen l_B, a different number of tethers is required to obtain the desired thrust energy. For example, two tethers with δ = 3.2 or four tethers with δ = 4.4 can be chosen, if l_B = 1.0. The total tethers mass weakly depends on the number of tethers (0.62 MT and 0.60 MT respectively), but the required total tether length for those cases is very different, about 30 km for δ = 3.2, and ~80 km for δ = 4.4. The total MXER facility length is about 80 km, and the choice of δ = 4.4 or larger will require a parallel tether design.

[19] For the tape geometry, as can be seen from Figures 3b and 3c, for the given δ the permitted l_B are restricted from the side of larger l_B by the OML applicability condition ($h + d \leq 4\lambda_D \approx 1$ cm). From the side of smaller l_B the restriction is because these l_B and the bare segment length, l_b, (green curves at the Figure 2) result in a cross section to perimeter ratio (expressions (3)) that leads to the cross-sectional area collecting currents larger than the permitted current. The OML regime of current collection applicability also restricts the permitted δ for a prescribed l_B, voltage, and current. The normalized work (black curves in Figures 4b and 4c) and the tether mass for the tape are close for different δ and the same l_B, so, the curves for the normalized work are shifted along the y-axes at the intervals in the parentheses. This makes clear the domain of the available l_B. Just as it is for the circular tethers, the normalized work is smaller than unity and facility reboost during the prescribed time (100 days) with only the help of one tether is impossible. However, depending on the choice of circular or rectangular cross section the number of tethers and the total length needed to obtain the required work (normalized work equal one) can be chosen differently. Consider circular and rectangular tethers with δ = 5. (As can be seen from Figure 2 for larger δ, tether performance is not too different.) Consider l_B = 1 and l_B = 1.3 corresponding to different electric power efficiency and system mass. For l_B = 1 the tether radius is prescribed by the choice of δ and l_B. For current collected by a circular tether this is about 11A (Figure 3a), and requires six tethers with a total length of $L \sim 90$ km (Figure 4a). For l_B = 1.3 it should be 16 tethers and in total, more than 200 km long. For a tape tether for a chosen δ and l_B, different cross sections can still be taken. With a cross section resulting in 25A of current, 3 tethers with a total length of about 40 km are required to obtain the needed work for both l_B (Figure 4b). Note that this length will still be about the facility length (80 km) for reboost times a factor of two shorter (which are desirable) than used in the thrust work normalization. The total length for the tape cannot be arbitrarily small, because the current should be collected in the OML regime. As can be seen from Figures 3c and 4c, the tethers discussed above for δ = 5 and l_B = 1, 1.3 are not available with a cross section needed to collect 50A of current.

[20] The applicable conditions for OML regime current collection imposed above can be less restrictive with some reduction in the current collection that is required (coefficient G in equation (2) smaller than one) [*Sanmartin and Estes*, 1999; *Estes and Sanmartin*, 2000].

[21] Because the currents required for MXER tether operation are large and the induced magnetic fields are large compared to the ambient magnetic field in the vicinity of the tether, we also studied the possible role of magnetic shielding (equations (3) and (4)). Tethers with a circular cross section (radius up to 0.3 cm) and tapes with cross sections up to 0.06 cm^2 and a thickness of 0.02 cm with limitations on the bare segment lengths of 20 km and 10 km, respectively, have been considered for currents up to 50A. It has been found that magnetic shielding is negligible for an equatorial, elliptical orbit. It should be noted that this will not always be the case and the effect essentially depends on the specifics of the mission. If inclined orbits for the MXER tether were to be used, as in the following example, then the role of magnetic shielding may not be negligible. The angle between the tether and the ambient magnetic field in this example is taken not at 90°, as in the calculations above, but at 30°. The effect of shielding for such a trajectory is presented in Figure 5. The results of this study are based on the model of magnetic shielding of *Khazanov et al.* [2000, 2001]. Similar results for this effect also follow from the model developed by *Sanmartin and Estes* [2002].

[22] The reasons for the difference between these orbits in regard to the magnetic shielding are in short as follows. Starting from the bare tether end the size of the plasma sheath and the region of the closed magnetic field surfaces around the tether are growing functions of the length along

the tether. Initially the plasma sheath grows faster than the domain of closed magnetic surfaces, then the opposite holds true. Both models assume that magnetic shielding manifests if the length of the separatrix enveloping closed magnetic field lines is larger than the length of the plasma sheath, i.e., the plasma sheath is inside the region of closed magnetic surfaces. Under this condition only a part of the thermal flux at the separatrix is able to reach the plasma sheath and will be collected by the tether. The coefficient $\varepsilon(l)$ in equations (4) is the ratio of these two fluxes (collected to incoming on the separatrix). The practical role of magnetic shielding depends on the length of the bare tether segment, current and voltage at the point along the tether, where the lengths of the separatrix and plasma sheath become equal, the tether segment length where this point is reached, L_{eq}, and the coefficient $\varepsilon(l)$ after this point. The separatrix length is proportional to $I/\sin\psi$, where ψ is the angle between the tether and the ambient magnetic field. The length of the plasma sheath is proportional to $\sqrt{\Delta V}$. From these it follows, with the help of the expressions (3), (5), (6), and $E_m \propto \sin\psi$, that L_{eq} and the corresponding current, at the point where the lengths of the separatrix and the plasma sheath are equal, are approximately proportional to $\sin\psi$, and $\sin^2\psi$, respectively, if the normalized current i is not too large. For the case presented in Figure 5, the numerical calculations for $\psi = 30^\circ$ leads to $L_{eq} = 2.5$ km, $I_{eq} = 15.2\,A$ and to $L_{eq} = 5.2$ km, $I_{eq} = 66A$ for $\psi = 90^\circ$ (equatorial orbit). So in the last case the current needed for the shielding is larger than the allowed current (50A). The corresponding coefficients in equation (4) are $\varepsilon = 0.17$ and 0.32 for the 10 km bare segment length. Therefore small angles between the tether and the Earth's magnetic field strongly act in favor of the magnetic shielding effects. The possible role of magnetic shielding should be considered in the context of other mission requirements for nonequatorial trajectories.

[23] We have considered partly insulated circular and tape tethers as thrusters for the MXER tether operational concept, for an equatorial elliptical orbit with perigee and apogee at the altitudes 300 km and 8500 km, respectively. It has been assumed that the electric source voltage is limited by 5 kV and the tether operates under zero potential bias at the bare segment end.

[24] The orbit-average electric power efficiency, the ratio of thrust related mass to the thrust times mission duration time, and the normalized thrust power have been calculated as functions of the ratio of bare to insulated segments length and of the cross-section parameters. Currents up to 50A for a circular cross section, and 25A and 50A currents for the tape and correspondingly available tether parameters have been considered. We also calculated the thrust work for these cases in relation to the work required to reboost the MXER facility during the prescribed time for a prescribed payload mass (2.5 MT) and the tether mass. It is found that more than one tether is needed if this time is taken to be 100 days.

[25] The use of electrodynamic tethers with a circular cross section requires a total tether length much larger than the currently expected length of the MXER facility for the required payload acceleration or a multiple tether design is needed. In contrast, a tape cross section can achieve the required reboost during less than the required time with the anticipated tether length. It has been found that for the planned equatorial orbit the effect of magnetic shielding is negligible, while it should be included in the analyses for orbits with significant inclination.

[26] Calculated results along the planned MXER tether trajectory can be used for the preliminary analyses of the tether performance and the choice of the preferable technology for system restoration.

[27] **Acknowledgments.** The work described in this paper was funded in part by the In-Space Propulsion Technology Program, which is managed by NASA's Science Mission Directorate in Washington, D. C., and implemented by the In-Space Propulsion Technology Office at Marshall Space Flight Center in Huntsville, Alabama, under the Technical Task Agreement M-ISP-04-37. The program objective is to develop in-space propulsion technologies that can enable or benefit near and midterm NASA space science missions by significantly reducing cost, mass or travel times.

[28] Arthur Richmond thanks the reviewers for their assistance in evaluating this paper.

References

Ahedo, E., and J. R. Sanmartin (2002), Analysis of bare-tether systems for deorbiting low-Earth orbit satellites, *J. Spacecr. Rockets*, *39*, 198.

Estes, R. D., and J. R. Sanmartin (2000), Cylindrical Langmuir probes beyond the orbital motion limited regime, *Phys. Plasmas*, *7*, 4320.

Estes, R. D., E. C. Lorenzini, and J. R. Sanmartin (2002), Short tethers for electrodynamic thrust, in *Space Technology and Applications International Forum 2002*, edited by M. S. El-Genk, p. 548, Am. Inst. of Physics, New York.

Hoyt, R. P. (2000), Design and simulation of a tether boost facility for LEO → GTO payload transport, paper presented at 36th Joint Propulsion Conference, Am. Inst. of Aeronaut. and Astronaut., Huntsville, Ala., July.

Hoyt, R. P., J. T. Slostad, and S. S. Frank (2003), A modular Momentum-Exchange/Electrodynamic-Reboost tether system architecture, paper presented at 39th Joint Propulsion Conference, Am. Inst. of Aeronaut. and Astronaut., Huntsville, Ala., July.

Khazanov, G. V., N. H. Stone, E. N. Krivorutsky, and M. W. Liemohn (2000), Current-produced magnetic field effects on current collection, *J. Geophys. Res.*, *105*, 15,835.

Khazanov, G. V., N. H. Stone, E. N. Krivorutsky, K. V. Gamauynov, and M. W. Liemohn (2001), Current-induced magnetic field effects on bare tether current collection: A parametric study, *J. Geophys. Res.*, *106*, 10,565.

Sanmartin, J. R., and R. D. Estes (1999), The orbital motion limited regime for cylindrical Langmuir probes, *Phys. Plasmas*, *6*, 395.

Sanmartin, J. R., and R. D. Estes (2002), Magnetic self-field effects on current collection by an ionospheric bare tether, *J. Geophys. Res.*, *107*(A11), 1335, doi:10.1029/2002JA009344.

Sanmartin, J. R., M. Martinez-Sanchez, and E. Ahedo (1993), Bare wire anodes for electrodynamic tethers, *J. Propul. Power*, *9*, 353.

Sanmartin, J. R., R. D. Estes, and E. C. Lorenzini (2001), Efficiency of different types of ED-tether thrusters, in *Space Technology and Applications International Forum 2001*, edited by M. S. El-Genk, p. 479, Am. Inst. of Phys., New York.

Sorensen, K. (2003), Momentum eXchange Electrodynamic Reboost (MXER) Tether, final report, Technol. Assess. Group, NASA Marshall Space Flight Cent., Huntsville, Ala.

Stone, N. H., J. D. Moore, W. R. Clayton, and P. A. Gierow (2002), A preliminary assessment of grid-spheres used as end-body electrodes for electrodynamic tether, in *Space Technology and Applications International Forum 2002*, edited by M. S. El-Genk, p. 537, Am. Inst. of Phys., New York.

Vannaroni, G., M. Dobrowolny, and F. De Venuto (2000), Deorbiting of LEO satellites with electrodynamic tethers, paper presented at 38th Aerospace Sciences Meeting and Exhibit, Am. Inst. of Aeronaut. and Astronaut., Reno, Nev.

D. L. Gallagher and G. V. Khazanov, NASA Marshall Space Flight Center, Huntsville, AL 35805, USA.

E. N. Krivorutsky, Universities Space Research Association, National Space Science and Technology Center, Huntsville, AL 35805, USA. (george.khazanov@msfc.nasa.gov)